Electrowetting-Induced Droplet Movement in an Immiscible Medium

Jason S. Kuo, Paolo Spicar-Mihalic, Indalesio Rodriguez, and Daniel T. Chiu*

Department of Chemistry, University of Washington, Seattle, Washington 98195-1700

Received August 6, 2002. In Final Form: October 29, 2002

This paper describes and characterizes the electrowetting-induced movement of droplets in an immiscible medium. When an aqueous droplet undergoes electrowetting-induced motion in a continuous phase of olive oil, the droplet glides through the olive oil at a much higher velocity than is possible in the absence of oil and is able to travel greater than 10 times the electrode separation distance. To describe this behavior, a simple hydrodynamic model is developed to predict the droplet speed and to elucidate the mechanism of droplet movement. On the basis of this model, we also discuss a strategy to reduce droplet splitting.

Introduction

As the characteristic dimension of fluid flow is reduced to the micrometer range, surface energy becomes an increasingly important factor in determining the flow behavior. Because the surface-to-volume ratio is inversely proportional to the width of a channel, forces that arise from surface tension will become comparable to the inertial force of the fluid at a sufficiently small length scale. At this point, it becomes possible to manipulate the motion of the fluid or fluid droplet by modulating the surface tension, which can be achieved with a number of strategies, including the use of light,[1,2] temperature gradients,[3,4] electric field,[5−7] electrochemical methods,[8] and direct patterned surface modifications.[9−11] For microfabricated systems, the use of electric field to control dynamically the wetting properties of the surface provides a particularly versatile and convenient approach.[12−15] By burying metal electrodes underneath selected dielectric materials,[16−18] a circuit can be devised easily and rapidly for manipulating fluid droplet movement using this electrowetting effect.[19−23]

Electrowetting has its unique virtues when compared to other methods of transporting fluids in micrometer-sized channels. Although the ultimate flow velocity that can be achieved is nowhere as high as that with pressure-driven flow, electrowetting has been shown to produce consistently droplet velocities on the order of centimeters/second, as reported in ref 12 and later in this paper. This velocity range is very reasonable for typical lab-on-a-chip applications and is higher than the typical velocities obtainable with electro-osmotic flow.[24] In addition, electrowetting also offers exquisite control over the direction of fluid movement and allows manipulation of discrete droplets inside of another immiscible fluid medium. This can be used, for example, to design microfluidic-based optical switches or other photonic components.[25,26]

Despite the wide range of potential applications for electrowetting-based fluid manipulation, there have been no detailed studies on the behavior of droplet movement in an immiscible fluid medium. This paper investigates the electrowetting-induced motion of an aqueous droplet encapsulated in an immiscible fluid, and presents a model that accounts for the hydrodynamic fluid response to describe this droplet movement. We found the presence of an immiscible fluid provides lubrication and permits faster droplet motion as well as longer travel distance for the droplet. On the basis of this model, we also discuss a strategy to reduce droplet splitting. For the dielectric material used in electrowetting, we chose a poly(dimethylsiloxane) (PDMS) coated surface. While PDMS is well-known in the electronics industry as an excellent sealant and encapsulant for high voltage applications ($\epsilon = 2.75$; dielectric strength of 21 kV/mm), it is also a material commonly encountered in microfluidics for molding microchannels.[27,28] Like fluoropolymers commonly used in previous electrowetting reports,[16] PDMS is intrinsically

* To whom correspondence should be addressed.

(1) Ichimura, K.; Oh, S. K.; Nakagawa, M. *Science* **2000**, *288*, 1624−1626.
(2) Wang, R.; Hashimoto, K.; Fujishima, A. et al. *Nature* **1997**, *388*, 431−432.
(3) Kataoko, D. E.; Troian, S. M. *Nature* **1999**, *402*, 794−797.
(4) Sammarco, T. S.; Burns, M. A. *Am. Inst. Chem. Eng. J.* **1999**, *45*, 350−366.
(5) Quillet, C.; Berge, B. *Curr. Opin. Colloid Interface Sci.* **2001**, *6*, 34−39.
(6) Colgate, E.; Matsumoto, H. *J. Vac. Sci. Technol. A* **1990**, *8*, 3625−3633.
(7) Rosslee, C.; Abbott, N. L. *Curr. Opin. Colloid Interface Sci.* **2000**, *5*, 81−87.
(8) Gallardo, B. S.; Gupta, V. K.; Eagerton, F. D.; Jong, L. I.; Craig, V. S.; Shah, R. R.; Abbott, N. L. *Science* **1999**, *283*, 57−60.
(9) Daniel, S.; Chaudhury, M. K.; Chen, J. C. *Science* **2001**, *291*, 633−636.
(10) Zhao, B.; Moore, J. S.; Beebe, D. J. *Science* **2001**, *291*, 1023−1026.
(11) Gleiche, M.; Chi, L. F.; Fuchs, H. *Nature* **2000**, *403*, 173−175.
(12) Pollack, M. G.; Fair, R. B.; Shenderov, A. D. *Appl. Phys. Lett.* **2000**, *77*, 1725−1716.
(13) Lee, J.; Moon, H.; Fowler, J.; Schoellhammer, T.; Kim, C. J. *Sens. Actuators, A* **2002**, *95*, 259−268.
(14) Lee, J.; Kim, C. J. *J. Microelectromech. Syst.* **2000**, *9*, 171−180.
(15) Ding, H.; Chakrabarty, K.; Fair, R. B. *IEEE Trans. Comput.-Aided Des. Integr. Circuits Syst.* **2001**, *20*, 1463−1468.
(16) Seyrat, E.; Hayes, R. A. *J. Appl. Phys.* **2001**, *90*, 1383−1386.
(17) Vallet, M.; Berge, B.; Vovelle, L. *Polymer* **1996**, *37*, 2465−2470.
(18) Sondaghuethorst, J. A. M.; Fokkink, L. G. J. *Langmuir* **1994**, *10*, 4380−4387.
(19) Decamps, C.; De Coninck, J. *Langmuir* **2000**, *16*, 10150−10154.
(20) Verheijen, H. J. J.; Prins, M. W. J. *Langmuir* **1999**, *15*, 6616−6620.
(21) Vallet, M.; Vallade, M.; Berge, B. *Eur. Phys. J. B* **1999**, *11*, 583−591.
(22) Digilov, R. *Langmuir* **2000**, *16*, 6719−6723.
(23) Peykov, V.; Quinn, A.; Ralston, J. *Colloid Polym. Sci.* **2000**, *278*, 789−793.
(24) McKnight, T. E.; Culbertson, C. T.; Jacobson, S. C.; Ramsey, J. M. *Anal. Chem.* **2001**, *73*, 4045−4049.
(25) Mach, P.; Krupenkin, T.; Yang, S.; Rogers, J. A. *Appl. Phys. Lett.* **2002**, *81*, 202−204.
(26) Berge, B.; Peseux, J. *Eur. Phys. J. E* **2000**, *3*, 159−163.
(27) McDonald, J. C.; Duffy, D. C.; Anderson, J. R.; Chiu, D. T.; Wu, H.; Whiteside, G. M. *Electrophoresis* **2000**, *21*, 27−40.

10.1021/la020698p CCC: $25.00
Published on Web 12/14/2002

extremely hydrophobic. It is, however, only at a small fraction of the cost of Teflon, which makes PDMS an attractive material for integration into electrowetting-based devices.

Theory of Electrowetting

Electrowetting is a phenomenon that relates changes in surface interfacial energy with the presence of an electric field. As an electric field is applied through a dielectric material, a liquid droplet above the dielectric surface experiences a change in surface interfacial energy and thus a change in the droplet's equilibrium contact angle. Typically the presence of the electric field results in a reduction of surface interfacial energy and hence the contact angle. The characteristic response of a droplet can be described by the Lippmann−Young equation.[29] For generality, the equation is modified to assume that the interaction between solid/vapor and solid/liquid is nonzero:

$$\cos\theta = \frac{(\gamma_{s\beta} - \gamma_{s\alpha})}{\gamma_{\alpha\beta}} + \frac{1}{2\gamma_{\alpha\beta}}\frac{\epsilon_0\epsilon}{d}V^2 \qquad (1)$$

where γ_{ij} refers to the surface interfacial energy between phases as identified by the subscripts (α = droplet, β = surrounding medium, which may be liquid or gas, and s = solid substrate). ϵ and d refer to the dielectric constant and the thickness of the solid surface above the electrode, and V is the applied voltage. Not all systems, however, obey the quadratic reduction of surface energy under applied electric field. A single decane droplet immersed in water on a perfluoroalkoxy (Hostaflon-PFA) surface, for example, exhibited a linear, antisymmetric response with respect to applied voltage.[29] Although deviation from the Lippman−Young equation in some instances may be attributed to surface effects such as surface charge accumulation or surface morphology, increasing experimental evidence indicates that the equation may be too simplified to account for the vast combinations of substrates and fluids.

For a microdroplet sitting on top of an embedded electrode (Figure 1A), the surface interfacial energy is a result of interactions between the surface (phase s) and the surrounding medium (phase β), the surface and the liquid drop (phase α), and the liquid drop and the surrounding medium. The balance of surface tension can be written as

$$\gamma_{s\beta} = \gamma_{s\alpha} + \gamma_{\alpha\beta}\cos\theta \qquad (2)$$

To generate flow using electrowetting, a gradient of or a change in surface interfacial energy must be created along the path of the droplet movement. This change is accomplished typically by burying discrete, individually addressable electrodes orthogonal to the path of droplet motion. Figure 1B is a schematic of the side view of a droplet placed inside a channel, which shows four contact angles from which one can write a force balance between the inside of the droplet (phase α) and the surrounding medium (phase β):[13]

$$P_R - P_\beta = -\frac{(\gamma_{\alpha\beta}\cos\theta_{top} + \gamma_{\alpha\beta}\cos\theta_{bot})}{2R} \qquad (3)$$

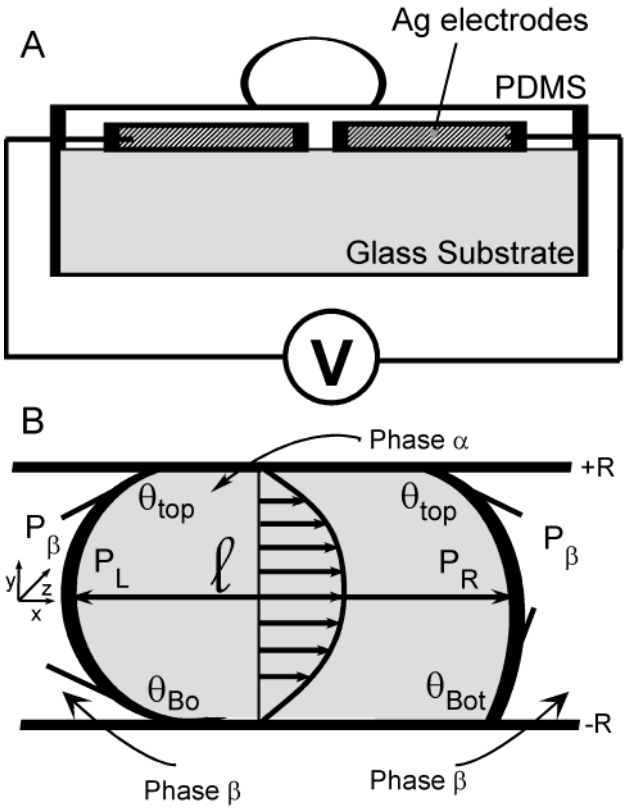

Figure 1. (A) Schematic depicting the experimental arrangement of the electrodes. (B) Coordinates and dimensions used in the mathematical modeling of droplet movement. The application of a voltage to the electrodes underneath the droplet creates a difference between the left−bottom and right−bottom contact angles (θ_{Bo} and θ_{Bot}), which induces a pressure differential across the droplet. This pressure differential initiates a flow, which can be described by the Navier−Stokes equation, until the droplet moves across the electrode gap.

and

$$P_L - P_\beta = -\frac{(\gamma_{\alpha\beta}\cos\theta_{top} + \gamma_{\alpha\beta}\cos\theta_{Bo})}{2R} \qquad (4)$$

Equations 3 and 4 can be combined into

$$P_L - P_R = \frac{\gamma_{\alpha\beta}(\cos\theta_{Bot} - \cos\theta_{Bo})}{2R} \qquad (5)$$

Equation 5 describes a net internal pressure, as a result of the changes in contact angle, which pushes the fluid droplet from left to right. The exact functional dependence of $\cos\theta_{Bot} - \cos\theta_{Bo}$ on electric field depends on many parameters. And as mentioned earlier, the change in contact angle does not always obey the Lippman−Young equation. For generality, we will treat the functional dependence as a constitutive equation that is specific to the combination of substrate and fluids chosen:

$$\cos\theta_{Bot} - \cos\theta_{Bo} = f(V,d,\epsilon,\gamma_{s\alpha},...) \qquad (6)$$

in which the value of $f(V,d,\epsilon,\gamma_{s\alpha},...)$ must be less than 1 and the exact functional dependence on applied voltage is subject to the substrate/fluid combination.

From the difference in net internal pressure (eq 5), we can compute the internal velocity profile and estimate the droplet velocity by solving the Navier−Stokes equation subject to the appropriate boundary conditions. Building

(28) Unger, M. A.; Chou, H. P.; Thorsen, T.; Scherer, A.; Quake, S. R. *Science* **2000**, *288*, 113−116.

(29) Janocha, B.; Bauser, H.; Oehr, C.; Brunner, H.; Göpel, W. *Langmuir* **2000**, *16*, 3349−3354.

upon Huang et al.'s[30] and Barraza et al.'s[31] analyses of the velocity profile due to capillary effects, we present a simple model to provide a theoretical framework for electrowetting-driven droplet movement so as to elucidate the fundamental hydrodynamic forces involved.

The internal flow of the droplet can be described with the Navier−Stokes equation

$$\frac{\partial \vec{v}}{\partial t} + (\vec{v}\cdot\nabla)\vec{v} = \frac{1}{\rho}\nabla P + \frac{\mu}{\rho}\nabla^2\vec{v} \tag{7}$$

and the continuity equation

$$\nabla\cdot\vec{v} = 0 \tag{8}$$

We assume that the fluid is incompressible and Newtonian and that no external force, such as gravity, is acting on the fluid. Because the electrodes used in electrowetting are placed only along the path of droplet movement, we can assume with reasonable approximation that the flow is only in one dimension, that is, toward the activated electrode. Therefore, the pressure gradient supplied by the electrowetting phenomenon is

$$\nabla P = \frac{\Delta P}{l} = \frac{2\gamma_{\alpha\beta} f(V,d,\epsilon,\gamma_{s\alpha},...)}{l^2} \tag{9}$$

where l is the droplet diameter, which may vary with time, since electrowetting changes the contact angle. For simplification, we also assumed that the droplet is approximately spherical (i.e., $2R \approx l$). $\gamma_{\alpha\beta}$ denotes the surface tension between two fluid phases, and in the case of a droplet of phase α surrounded by gas, $\gamma_{\alpha\beta}$ is simply γ_α, the surface tension of liquid α as commonly tabulated in handbooks. The factor of 2 in eq 9 is included to account for two convex surfaces. Because we are only interested in the overall droplet velocity, it is not of particular interest to solve for the three-dimensional spatial velocity profile. We can, therefore, integrate the Navier−Stokes equation over the directions orthogonal to the flow direction to get a spatial "average" velocity:

$$2RW\frac{\partial V_{avg}}{\partial t} = \frac{2RW}{\rho}\,\frac{2\gamma_{\alpha\beta} f}{l^2} + \frac{\mu}{\rho}W\left(\frac{\partial v_x}{\partial y}\right)_{-R}^{R} \tag{10}$$

where W is the channel dimension in the z direction. To further approximate, we assume a typical parabolic flow profile for v_x:

$$v_x = \frac{3}{2}V_{avg}\left[1 - \left(\frac{y}{R}\right)^2\right] \tag{11}$$

This approximation is reasonable, based on the demonstration by Huang et al. that the velocity profile is Poiseuillean at a distance far enough away from the meniscus. Assuming $V_{avg} = \partial l/\partial t$, that is, the average velocity is equal to the rate of the expansion and contraction of the droplet diameter, one arrives at the following differential equation:

$$\frac{\partial^2 l}{\partial t^2} + \frac{3\mu}{\rho R^2}\,\frac{\partial l}{\partial t} - \frac{2\gamma_{\alpha\beta} f}{\rho l^2} = 0 \tag{12}$$

subject to the initial conditions that $l(0)$ is equal to the initial droplet size and that $l'(0)$, the initial droplet velocity, is zero. Equation 12 can be solved numerically. Because the velocity induced by electrowetting is quite fast, the droplet can clear the separation gap in as short as 0.01 s. After clearing the gap, the droplet no longer possesses the internal pressure gradient and can only travel with the imparted momentum. The calculation of droplet velocities presented in Figure 4 takes into account this sudden drop in driving force and computes a time-averaged velocity for comparison with our experimental measurements.

Experimental Section

Microfabrication. Glass microscope slides (50 mm × 70 mm) were degreased either by sonication for 5 min in acetone and then for another 5 min in methanol or by boiling in a solution of NH_4OH, H_2O_2, and H_2O in a 2:2:3 ratio for 60 min. After degreasing, the slides were dried under a stream of N_2 gas. Ag electrodes were deposited onto the surface by flowing electroless Ag plating solutions through PDMS microchannels that have been conformally sealed onto the glass surface. The master used for molding PDMS microchannels was prepared using photolithography and has been described in detail elsewhere.[27] The Ag patterned glass slides were then annealed at 400 °C on a hot plate under N_2 for 90 min to promote adhesion. To form electrical connection to an external power supply, Cu braids were bonded to the electrodes using conductive epoxy (Chemtronics CW2400) cured in a 75 °C oven for at least 2 h.

Spin Coating of PDMS. PDMS (Sylgard 184, Dow Corning) was mixed at a 10:1 ratio (10 parts polymer and 1 part curing agent), rigorously stirred, and then vacuum outgassed for ∼45 min prior to spin coating. PDMS was first spread onto the electrodes at 500 rpm for 15 s, followed by coating at 2000 rpm for 30 s. The coated electrode assembly was then placed in the oven at 75 °C overnight to ensure thorough curing. The thickness of the spin-coated PDMS was measured using a Tencor Alpha Step 200 surface profilometer.

Electrowetting Setup. The electrode assembly was placed on a custom-built holder under a microscope and connected to a Stanford Research 1250V dc power supply (Sunnyvale, CA). A CCD camera was attached to the microscope to capture the droplet motion at 30 frames per second and store it onto videotapes. Droplet motion was studied both from the top and from the side by reorienting the microscope. A switching box was constructed to manually switch the output voltage to the desired electrode while grounding the remaining electrodes.

Results and Discussion

To evaluate PDMS as a candidate dielectric material for electrowetting applications, we first characterized the equilibrium contact angle of deionized water (DI), 100 mM aqueous KCl, and olive oil droplets on top of PDMS. As an illustration of the extent of electrowetting, Figure 2A shows successive frames of a droplet of KCl viewed from the side when no voltage was applied (left) and when −500 V was applied (right). Figure 2B plots the contact angles for each liquid as a function of the applied voltage. The thickness of the PDMS film on top of the electrode was 38 μm. At zero voltage, the contact angle of DI on PDMS was ∼102°, which is consistent with the reported literature values of 105° for the advancing edge and of 102° for the receding edge.[32] This contact angle is slightly less than that measured for Teflon, which has a contact angle near 115°.[16] We found that our experimental data fit much better to a linear model (i.e. linearly proportional to the absolute applied voltage) rather than the Lippman−Young relation. This again illustrates that while the quadratic dependence may be true for select substrates and fluids, the Lippman−Young relation must be open to

(30) Huang, W.; Bhullar, R. S.; Fung, Y. C. *J. Biomech. Eng.−T. ASME* **2001**, *123*, 446−454.

(31) Barraza, H. J.; Kunapuli, S.; O'Rear, E. A. *J. Phys. Chem. B* **2002**, *106*, 4979−4987.

(32) Hillborg, H.; Ankner, J. F.; Gedde, U. W.; Smith, G. D.; Yasuda, H. K.; Wikstrom, K. *Polymer* **2000**, *41*, 6851−6863.

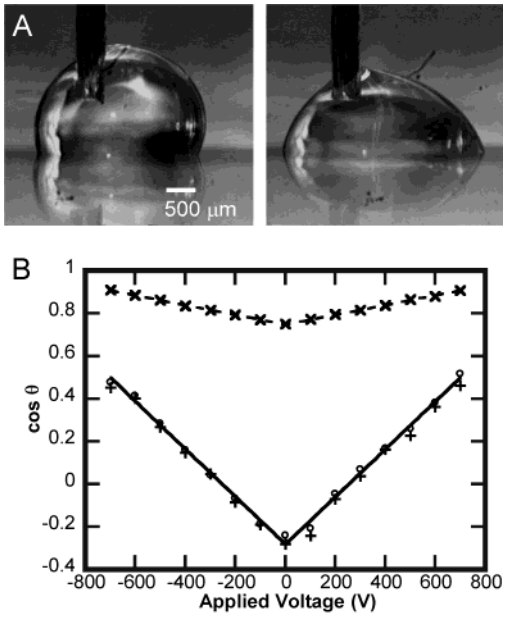

Figure 2. (A) Before (left) and after (right) the application of −500 V that causes the 100 mM KCl droplet to flatten out. (B) Equilibrium contact angle measurements for DI water (○), 100 mM KCl (+), and olive oil (×). Virtually no difference was observed in the electrowetting behaviors of DI water and 100 mM KCl. To perform the measurement, the droplet is placed on top of a disk-shaped electrode with a 38-μm thick PDMS layer spun coated on top. A grounding electrode is inserted into the droplet to complete the circuit.

modification for different combinations of substrates and fluids to account for possible mechanistic effects.

To study the effect of the presence of an immiscible fluid, we suspended a droplet of 100 mM KCl in olive oil. Figure 3A shows successive frames of KCl droplet motion upon application of a voltage. Originally suspended near the top of olive oil, the KCl droplet (arrow) rapidly moved toward the electrode separation gap when −500 V was applied, and then it flattened out onto the dielectric surface and was "slingshot" out toward the negatively biased electrode. The flattening motion and the characteristic change in contact angle can be observed in the third frame (66 ms) of Figure 3A. This flattening confirms that the motion of the KCl droplet was not caused by electrostatic attraction or repulsion (e.g., ion migration).

We recognize that the olive oil composition can vary significantly depending on the blend, origin, and extraction technique. We examined several other immiscible fluids before we narrowed the selection down to olive oil. Paraffin oil (e.g., from VWR mechanical pump fluid) exhibited good electrowetting behavior, but it is not as quick as that of olive oil. Other organic fluids often penetrated into the thin PDMS dielectric layer and caused swelling or dielectric breakdown, or exhibited no response at all. This observation again illustrates the role of fluid−substrate interaction in dynamic electrowetting, which is not addressed in the conventional Lippman−Young relation. Olive oil data are presented because of its dramatic response and surface compatibility.

Figure 3B shows the simulated velocity trace of the droplet as predicted by our hydrodynamic model. Consistent with our experimental observation, the initial droplet velocity increased rapidly due to the build up of the internal pressure gradient. This pressure increase is counterbalanced by the viscous response of the fluid, which begins to dominate at longer time scales. The velocity trace plotted in Figure 3B, however, does not include the

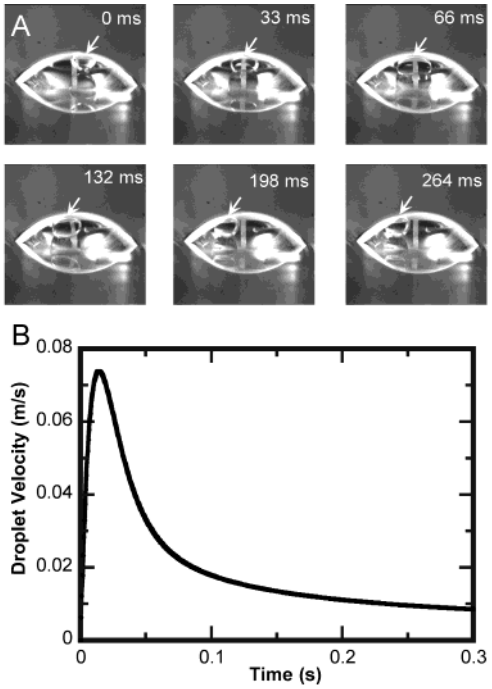

Figure 3. (A) Successive frames of a 100 mM KCl droplet undergoing electrowetting motion in a larger drop of olive oil. The KCl droplet is initially suspended near the top center of the encapsulating olive oil. As voltage (−500 V to the electrode placed at the left) is applied, the droplet flattens near the surface and moves across the electrode gap. (B) Simulated velocity trace of droplet motion at −500 V. The initial sharp increase in velocity is caused by electrowetting-induced pressure buildup. As time progresses, the droplet expands across the electrode, which reduces the pressure gradient that drives the droplet. At this voltage, the droplet should clear the gap in ∼0.9 ms after the change in contact angle has occurred, according to this model.

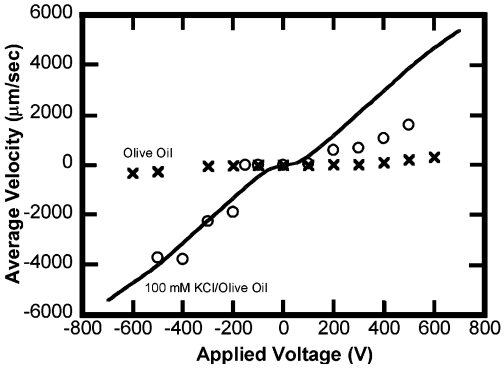

Figure 4. Plot of the average droplet velocity as a function of applied voltage. The experimental measurements are indicated by (×) for olive oil and by (○) for 100 mM KCl in olive oil. The line drawn through the measurements for KCl in olive oil (○) is the simulated velocity using our model.

fact that in our experiments the droplet would have cleared the electrode gap before it could reach the maximum predicted velocity. Once the droplet cleared the gap, the electrowetting-induced pressure gradient suddenly disappeared, causing the droplet to decelerate immediately in the presence of viscous force until it stopped. Experimentally observed deceleration, therefore, should have occurred sooner than predicted in Figure 3B.

Figure 4 shows a plot of the measured time-averaged droplet velocity as a function of applied voltage. The measurement was performed in an enclosed microchannel (Figure 1B). For a KCl droplet suspended in olive oil, the velocity simply increases as a function of voltage, reaching

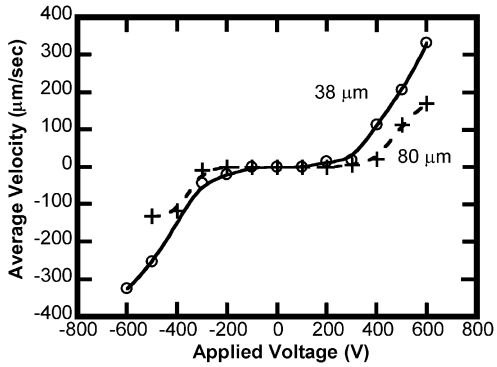

Figure 5. Dependence of the velocity of an olive oil droplet on the thickness of the spin coated PDMS film.

almost 3.5 cm/s at −500 V. For olive oil only, however, the droplet velocity begins at a relatively low value and increases monotonically and slowly at ∼300 V. The KCl droplet moves at ∼10 times the velocity in olive oil as compared with that of the olive oil droplet alone. Without olive oil, aqueous KCl moves even slower than the olive oil droplet alone. Since the difference due to the presence of olive oil is so drastic, we cannot attribute the observed velocity enhancement to the internal convection of olive oil induced by electrowetting. Rather, we ascribe this speed enhancement to the lubrication effect provided by olive oil. Instead of contacting a solid surface and consequently having to be subjected to the no-slip boundary condition imposed by the stationary surface, a KCl droplet hydroplanes in olive oil. The boundary condition imposed by the liquid−liquid interface only requires that the velocities of each phase are equal at the boundary and that the momentum transfer is continuous across the interface. Consequently, the solid−fluid frictional resistance is not experienced directly by the KCl droplet. The higher threshold voltage required to initiate olive oil droplet movement also implies the presence of friction at the surface.

The solid line drawn through the experimental measurements for the KCl/olive oil average velocity in Figure 4 is the simulated average droplet velocity calculated using our model. This average velocity is computed by calculating the time it takes for the drop to clear the electrode gap and then averaging the velocity trace over that period. Our model agrees well with our experimental data in the negative-voltage regime, but it overestimates it in the positive-voltage regime. Although the simulated velocities are symmetric with respect to both positive and negative voltages, experimentally the application of negative voltage induces faster droplet motion than that for positive voltage. This behavior is consistently observed throughout our experiments, albeit to a lesser extent in the olive oil only measurements. The exact nature of this polarity discrepancy has yet to be investigated, although several research groups have also reported similar observations with fluoropolymer substrates. Seyrat et al.[16] cited nanoporosity or the presence of oxygen atoms in a fluoropolymer structure as possible causes for the deviation in contact angle when applying a positive voltage bias. Janocha et al.[29] suggested that since certain polyfluorocarbon polymers are known to accumulate negative charge when immersed in water, the charge accumulation may alter the electric field line and reduce the positive voltage response. Although these are plausible explanations, they have not been examined in detail mechanistically.

Figure 5 illustrates the dependence of the droplet velocity on the thickness of PDMS, our dielectric material.

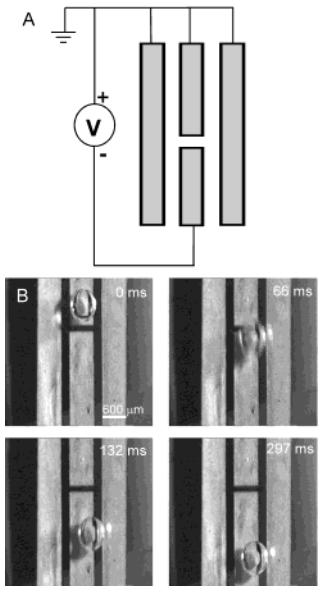

Figure 6. (A) Schematic of the electrode design used to demonstrate the gliding of a KCl droplet in olive oil. (B) Successive video frames showing the gliding of the KCl droplet with the application of −700 V to the bottom electrode.

The Lippman−Young equation accounts for variations in this thickness. As the PDMS layer becomes thinner, the change in contact angle becomes greater, which leads to a faster olive oil droplet velocity. Empirically, above a threshold voltage of ∼200 V, we observed the velocity to scale linearly as a function of applied voltage. We were unable to use reliably PDMS layers that are thinner than 38 μm using our procedure, due to frequent dielectric breakdown. This breakdown may be caused by defects, such as residual solvent or pores in the PDMS film. Several recent reports have observed that, by impregnating the dielectric with silicone oil or another nonpolar oil, the fluidic movement (low hysteresis in contact angle) is improved.[16,20] Verheijen[20] attributed this improvement to the penetration of silicone oil into the nanopores of the amorphous fluoropolymer layer, which reduces surface heterogeneity. With better quality thin PDMS films, we expect to obtain higher droplet velocities at a lower applied voltage.

By reducing friction, it is also possible to propel droplets farther than the separation gap between the electrodes. Figure 6 demonstrates this concept of "low-friction guide", in which a defined length of olive oil is placed on top of the PDMS-coated electrodes. In addition to the electrodes used for electrowetting, two side electrodes are introduced to guide the droplet to move in a straight path. When a voltage is applied to the electrodes, the KCl droplet undergoes electrowetting-induced flattening and is propelled toward the negative electrode. Once the droplet reaches the negative electrode, it continues to travel for at least 10 times the electrode separation distance. By incorporating these features, the droplet can move farther with a given pair of electrodes, and electrode design can be greatly simplified.

By inducing droplet motion in an immiscible medium rather than air, we can also minimize droplet splitting. Instead of moving toward the energized electrode, a droplet in air frequently splits into two smaller ones with the onset of an applied voltage, with each small droplet traveling in the opposite direction and at a higher velocity than is the case for the original drop. Figure 7 shows the energy changes involved in splitting a drop of phase α in an immiscible phase β into two smaller identical drops.

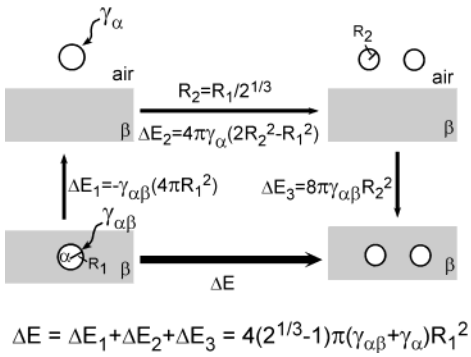

Figure 7. Schematic detailing the energy required to separate one droplet into two smaller identical droplets in an immiscible medium. As opposed to the case of separating the droplet in air, the presence of an immiscible medium increases the energy required to separate the droplet and thus reduces the tendency for droplet splitting.

The energy required to split the drop is given by

$$\Delta E = 4(\sqrt[3]{2} - 1)\pi(\gamma_{\alpha\beta} + \gamma_{\alpha})R_1^2 \qquad (13)$$

Equation 13 indicates that the energy involved in droplet splitting is controlled by the interfacial surface tension between the droplet and the immiscible medium ($\gamma_{\alpha\beta}$), the droplet surface tension with air (γ_{α}), and the initial diameter (R_1). By selecting an immiscible fluid having a high interfacial surface tension with the KCl droplet, the tendency for droplet splitting would be reduced. Hydrocarbons, which typically have an interfacial surface tension with water on the order of 50 mN/m,[33] are a good choice to stabilize the droplet movement.

Conclusions

The use of electrowetting to move an aqueous droplet in an immiscible medium offers two main advantages: (1) The immiscible medium can act as a lubrication layer, which significantly increases the velocity of droplet motion and the response of the system, and (2) the increased interfacial interaction between the aqueous droplet and the immiscible medium can prevent or minimize the splitting of the drop upon application of an electric field. Patterning immiscible fluids onto surfaces and using them as "low-friction guides" for directing droplet movement may find practical analytical applications, in which individual droplets can act as reaction vessels or as transporters of microsamples and reagents. With techniques of microfabrication, arrays of electrodes, patterned low-friction guides, and individual droplets can be created and applied toward the combinatorial recombination and sorting of the different contents contained within each droplet.

Acknowledgment. J.S.K. acknowledges partial support from the Joint Institute for Nanoscience funded by the Pacific Northwest National Laboratory (operated by Battelle for the U.S. Department of Energy) and the University of Washington. This research was funded by the Washington Technology Center (F01-PS2), by an ACS-PRF grant (37358-G), by the Research Corporation (RI0631), and by the Dreyfus Foundation (NF-00-077).

LA020698P

(33) Birdi, K. S. In *Handbook of Surface and Colloid Chemistry*; CRC Press: Boca Raton, FL, 1997; p 104.